JOURNAL OF APPLIED PHYSICS VOLUME 90, NUMBER 8 15 OCTOBER 2001

Polymorphous Si thin films from radio frequency plasmas of SiH_4 diluted in Ar: A study by transmission electron microscopy and Raman spectroscopy

G. Viera[a)] and S. Huet
Groupe de Recherche sur l'Energétique des Mileiux Ionisés (GREMI), BP 6744, Université d'Orléans, 45067 Orléans, Cedex 02, France

E. Bertran
Departments Física Aplicada i Òptica, Universitat de Barcelona, Avgda. Diagonal, 647, E08028 Barcelona, Spain

L. Boufendi
Groupe de Recherche sur l'Energétique des Mileiux Ionisés (GREMI), BP 6744, Université d'Orléans, 45067 Orléans, Cedex 02, France

(Received 19 March 2001; accepted for publication 10 July 2001)

In this study, we present a detailed structural characterization by means of transmission electron microscopy and Raman spectroscopy of polymorphous silicon (pm-Si:H) thin films deposited using radio-frequency dust-forming plasmas of SiH_4 diluted in Ar. Square-wave modulation of the plasma and gas temperature was varied to obtain films with different nanostructures. Transmission electron microscopy and electron diffraction have shown the presence of Si crystallites of around 2 nm in the pm-Si:H films, which are related to the nanoparticles formed in the plasma gas phase coming from their different growth stages, named particle nucleation and coagulation. Raman scattering has proved the role of the film nanostructure in the crystallization process induced "*in situ*" by laser heating. © *2001 American Institute of Physics.* [DOI: 10.1063/1.1398066]

I. INTRODUCTION

For several years, amorphous silicon films (*a*-Si:H) produced by plasma enhanced chemical vapor deposition have stimulated great interest in the microelectronics industry. This fact has led to numerous studies aiming to understand the formation process by plasma in order to obtain films with optimized optoelectronic properties. Amorphous silicon *a*-Si:H is a well-known material owing to its suitable optical and electronic transport properties and is now used not only in microelectronics, but also in various applications such as solar cells, liquid crystal displays, photocopiers, flat panel displays, and thin film transistors.[1]

In order to improve the characteristics of the films, i.e., to increase deposition rate and/or to improve film quality (transport and stability properties), plasma conditions have been widely explored. Frequently, the formation of powder particles has been observed in the plasma gas phase and considered as a source of contamination for the production of silicon based devices due to an enhancement of porosity, pinholes, and roughness. Thus, since the early 90's, many investigations have been aimed at understanding the silicon powder formation and its effects on the plasma properties.[2–4] These studies have led to very interesting results both from the scientific and the industrial point of view.[5] Recently, silicon films deposited under conditions close to those for powder-particle formation have revealed interesting new optoelectronic properties, in particular better transport and stability properties as compared to *a*-Si:H.[6–9] This new class of silicon thin films has been fabricated using a wide range of plasma conditions.[10–14] They are referred to as polymorphous silicon (pm-Si:H).[11,13–15] or as hydrogenated nanostructured Si (ns-Si:H).[12,16–18] These films are found to be constituted by an amorphous silicon matrix, in which ordered silicon domains with nanometer sizes (1–2 nm) are embedded.[12,13] Polymorphous silicon is now considered as a good candidate in possible future applications particularly in the photovoltaic domain.[8,13,14]

In this article, the structure and properties of polymorphous Si thin films deposited using Ar-SiH_4 low pressure modulated radio-frequency (rf) dusty plasmas are studied. The modulation period of the discharge and deposition temperature was varied to obtain films with different nanostructures. Morphological and structural analyses from transmission electron microscopy (TEM) and electron diffraction are reported. The presence of Si crystallites in the as-deposited films, as revealed by TEM, is found to facilitate the crystallization process induced by annealing, as studied "*in situ*" by Raman spectroscopy at increasing laser intensities on the samples. The threshold energy allowing the laser-induced amorphous-to-crystalline transition in these films was determined from the Raman analysis. The results obtained are correlated with the deposition plasma properties.

II. EXPERIMENTAL PROCEDURES

A. Film preparation

The experimental setup used in this work has already been described in detail elsewhere.[19] The radio-frequency

a)Electronic mail: gregorio.viera@univ-orleans.fr

 © 2001 American Institute of Physics

Downloaded 15 Jun 2010 to 161.116.168.169. Redistribution subject to AIP license or copyright; see http://jap.aip.org/jap/copyright.jsp

(13.56 MHz) discharge is produced in a grounded cylindrical box (13 cm inner diameter) equipped with a showerhead-type rf powered electrode. The bottom of the box is closed with a 20% transparency grid. This allows a vertical laminar gas flow. The discharge structure is surrounded by a cylindrical oven which allows the gas temperature to be varied from room temperature up to 200 °C. The gas temperature is measured in the gas flow below the bottom grid by means of a *J*-type thermocouple. Three vertical slits (2 mm width, 4 cm height) allow the optical access to the plasma at 0°, 90°, and 180° around the chamber. The whole system is enclosed in a vacuum vessel of 30 cm height and inner diameter. Three optical windows on the vacuum vessel (5 cm in diameter, placed 90° apart) are aligned with the slits. The experimental conditions used in this work were as follows: 30 sccm of Ar, 1.2 sccm of SiH_4, total pressure of 12 Pa and an rf power of 10 W corresponding to 600 V peak to peak.

The polymorphous silicon thin films are deposited using square-wave modulated discharges in SiH_4–Ar gas mixture with different duty cycles. The discharge is ignited for a given duration T_{ON} and then turned off for a fixed period T_{OFF} set to 1 s. During T_{ON} an amorphous Si film is deposited onto the substrate at the same time that nanoparticles nucleate in the plasma gas phase. During T_{OFF}, particles leave the plasma and are deposited onto the substrate. Consequently, after a great number of cycles, the final structure may consist of Si nanoparticles embedded in an amorphous matrix. The T_{OFF} period is chosen taking into account the residence time of the dust particles formed in the plasma which has been measured and found to be about 160 ms in the experimental conditions habitually used.[20] The thin layers studied were grown in well-known conditions in terms of particle nucleation and growth, which are: $0.1\ \mathrm{s} \leqslant T_{ON} \leqslant 5\ \mathrm{s}$ and a gas temperature $25\ ^\circ\mathrm{C} \leqslant T_G \leqslant 150\ ^\circ\mathrm{C}$. The substrates (stainless, Corning 7059 glass, *c*-Si wafer) were also chosen with respect to the different diagnostics used. The characteristics of the films studied in this work were compared to those of standard hydrogenated silicon films grown in SiH_4–H_2 plasmas at a substrate temperature of 250 °C.[21]

B. Film characterizations

High resolution transmission electron microscopy (HRTEM) micrographs and electron diffraction analysis were performed by means of a transmission electron microscope (Philips CM30) operating at 300 kV. The samples were cross sectionally prepared using the conventional preparation method. First, they were mechanically polished using abrasive materials and finally thinned with ion milling.

Raman scattering was used to investigate *in situ* the crystallization of the films. Raman spectra were recorded with a laser confocal micro-Raman spectrometer DILOR XY. The excitation was done by means of the 488 nm blue line of an Ar^+ laser. The laser beam can be focused on the surface sample by means of four different lenses corresponding to four different magnifications (×10, ×20, ×50, ×100). Thus the spot area can be varied from 1 up to 100 μm^2 and consequently the laser power density is varied from 0.35 up to 2000 kW/cm^2. All the spectra were referenced with those obtained on a *c*-Si measured under the same conditions. The Raman spectra were recorded during 300 s in order to have a good signal-to-noise ratio. The Raman measurements were first performed at the lowest power in order to avoid any thermal or induced effects such as crystallization of the samples. Then, the laser power density was gradually increased in order to determine the crystallization threshold.

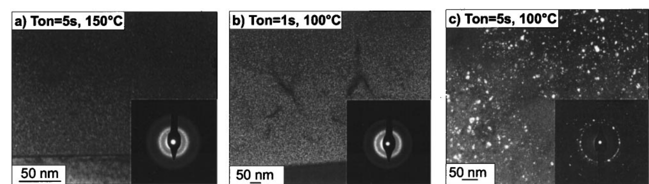

FIG. 1. Dark-field images of as-deposited pm-Si:H films grown in rf plasmas of Ar-diluted SiH_4 under different dust-forming conditions: (a) $T_{ON}=5$ s and $T_G=150$ °C; (b) $T_{ON}=1$ s and $T_G=100$ °C, and $T_{ON}=5$ s and $T_G=100$ °C. The inset in the images shows the corresponding selected area electron diffraction patterns.

The surface roughness of the films in their as-deposited state was determined by atomic force microscopy (AFM). These measurements were achieved using a Park Scientific Instrument microscope operating in air and contact mode. The results of roughness are considered in terms of root mean square values and are recorded on different scan areas [from (1×1) to (5×5) μm^2]. The roughness values presented in this study correspond to the average of that obtained for the different scan areas.

As-deposited thin film densities were deduced from the ratio of the weight to the volume of the layers. The weight of the deposited layers has been determined using a balance with a 1 μg accuracy.

III. RESULTS AND DISCUSSION

A. TEM characterization

TEM observations were performed on as-deposited pm-Si:H thin films grown under different experimental conditions. Figure 1 shows dark-field images of a thin film deposited at $T_{ON}=5$ s and at $T_G=150$ °C [Fig. 1(a)] and those of thin films deposited at the same lower temperature $T_G=100$ °C but at two different plasma durations [$T_{ON}=1$ s Fig. 1(b) and $T_{ON}=5$ s Fig. 1(c)]. In the inset of each image, the corresponding selected area electron diffraction (SAED) patterns are also shown. The SAED patterns of Figs. 1(a) and 1(b) contain diffuse rings which can be assigned to an amorphous structure. However, for the film obtained at $T_{ON}=5$ s and at $T_G=100$ °C, nanocrystalline features can be identified through the appearance of sharp rings. This pattern is different from the diamond-like structure of crystalline Si. After indexation, a face-centred-cubic (fcc) structure is revealed, as demonstrated by the appearance of the (111), (200), (220), (311), (331),..., diffraction rings. The lattice constant deduced from this diffraction pattern is 3.7 Å. A similar crystalline structure was found in nanostructured Si thin films deposited under continuous SiH_4–H_2 rf plasma[12] and in Si nanometric powder,[22] where nanocrystalline clusters with fcc structure were found to be embedded in an amorphous matrix.

Downloaded 15 Jun 2010 to 161.116.168.169. Redistribution subject to AIP license or copyright; see http://jap.aip.org/jap/copyright.jsp

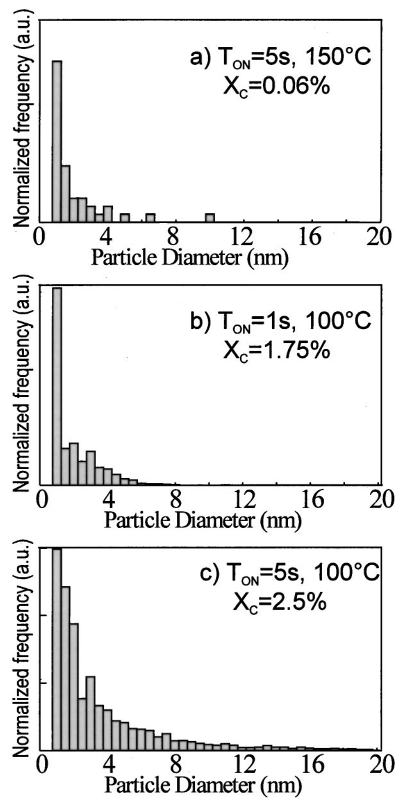

FIG. 2. Particle size histograms deduced from the TEM images on dark field of Fig. 1. The crystalline density (X_C) was also calculated from the dark-field images.

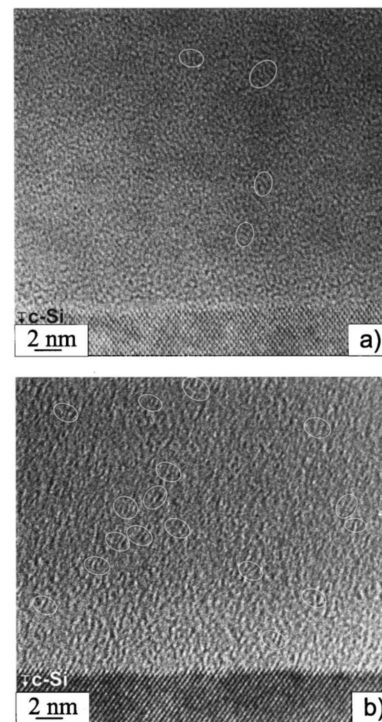

FIG. 3. HRTEM photographs of as-deposited pm-Si:H film deposited at $T_{ON}=5$ s and $T_G=150\,°C$ (a), and at $T_{ON}=1$ s and $T_G=100\,°C$ (b). Some of the nanometric ordered domains embedded in the amorphous silicon matrix are surrounded by a white line.

It is assumed that polymorphous Si films are formed by the incorporation of Si nanocrystallites (grown in the plasma gas phase) in an amorphous Si film. It is accepted that the metastable structure of small Si crystallites (~2 nm) is generally different from the bulk crystal.[23] These nanocrystallites may maintain the same atomic arrangement once incorporated into the film, thus leading to the peculiar crystalline structure of the polymorphous films as observed by electron diffraction.

There is no general agreement on the structure of the Si nanocrystallites which are only a few nanometers in size. Several authors have proposed different fullerene-like, cage-core or clathrates structures.[24–28] The cubic structure found in the Si crystallites containing pm-Si:H films could be compared to that of the Si clathrates. The clathrate structure consists of silicon polyhedra arranged to form a periodic structure.[29] In the center of some of these polyhedra there is a metal atom (Na, for example), which does not bond to any silicon atom, but which prevents the formation of the diamond cubic structure. The Si nanocrystallites generated by plasma have a similar structure to that of the clathrate polyhedra, but with H atoms which could play the same role as that of the metal atoms in the Si clathrates. Further research is now being undertaken to clarify the atomic structure of these polymorphous Si thin films.[30]

The dark-field images of the deposited film at $T_{ON}=5$ s and $T_G=100\,°C$ [Fig. 1(c)] clearly reveal a considerable increase in crystalline density, which is consistent with the emergence of distinct rings in the corresponding electron diffraction pattern. In order to obtain further information about the size and density of the crystallites in the different pm-Si:H samples, we have used an image processing and analysis software to identify the bright points in the dark-field images (considered as objects) and to extract the features of these objects (quantity, area, perimeter, roundness, etc.). By means of this software, the size histograms and the crystalline densities have been calculated (Fig. 2). These histograms indicate that the majority of crystallites present dimensions inferior to 2 nm, with decreasing populations for larger grain sizes. This figure also shows that crystalline density increases when the gas temperature decreases, and even more when plasma duration increases.

The lack of nanocrystalline-like diffraction for the sample deposited at $T_{ON}=1$ s [Fig. 1(b)] suggests that the pattern obtained from the sample deposited at $T_{ON}=5$ s [Fig. 1(c)] could correspond to the diffraction from the few larger grains of nearly 5 nm, which appear to present a much higher diffraction yield.

Figure 3 shows the HRTEM images of the thin film deposited at $T_{ON}=5$ s and at $T_G=150\,°C$ [Fig. 3(a)], and of the film deposited at $T_{ON}=1$ s and at $T_G=100\,°C$ [Fig. 3(b)]. The films deposited at higher temperature appear highly amorphous, while the sample deposited at 100 °C contains many ordered domains limited to 3–5 planes, corroborating the average crystallite size inferior to 2 nm calculated from the dark-field images (some of the ordered domains are surrounded by white circles in the image). The interplanar distances of these domains are 0.3–0.33 nm. A slightly larger interplanar distance is expected as compared to that of c-Si,

Downloaded 15 Jun 2010 to 161.116.168.169. Redistribution subject to AIP license or copyright; see http://jap.aip.org/jap/copyright.jsp

since the reduced size of these Si nanocrystallites allows a more relaxed crystalline structure. The HRTEM image of the sample deposited at 100 °C but at T_{ON}=5 s (not shown here) also showed the presence of these small crystalline entities, as well as of some larger crystallites up to 5 nm. These observations are commensurate with the results obtained from the dark-field images and do demonstrate the presence of ordered structures in the amorphous Si matrix of the films considered here. Comparable HRTEM images have already been reported for nanostructured Si thin films deposited using continuous rf discharges of SiH_4 highly diluted in H_2 at 100 °C and at low rf power.[12]

The plasma parameters for the production of these pm-Si:H films were adapted from previous reports devoted to the formation of silicon particles in Ar-diluted SiH_4 discharges.[20,31] Three growth phases in the particle formation have been defined: (i) a first step of nucleation of particles of around 2 nm, where particle concentration increases while their size remains constant; (ii) a second phase of coagulation of particles, which gives rise to bigger particles and to a drop in particle concentration; (iii) a third phase (from ~20–40 nm) where the coagulation is finished and particles grow more slowly by sticking of silicon radicals on their surface. These studies also showed that the gas temperature plays an important role in the process of particle formation, by delaying the appearance of the initial crystallites and, to a greater extent, the start of their coagulation.

Using the results of Boufendi *et al.*[20,31,32] we have estimated the characteristic times for the onset of particle nucleation (t_1), of coagulation (t_2) and of molecular sticking (t_3) for the three deposition temperatures considered in this study (T_G=25, 100, 150 °C), which are the following:

(i) T_G=25 °C: $t_1 \approx 0.001–0.01$ s, $t_2 \approx 0.15$ s, and $t_3 \approx 4$ s;
(ii) T_G=100 °C: $t_1 \approx 0.35$ s, $t_2 \approx 2$ s, and $t_3 \approx 13$ s; and
(iii) T_G=150 °C: $t_1 \approx 1$ s, $t_2 \approx 10$ s, and $t_3 \approx 20$ s.

In view of these results, the sample deposited at 150 °C and T_{ON}=5 s as well as the sample deposited at 100 °C and T_{ON}=1 s could contain only crystallites of a few nanometers coming from the first nucleation stage. This is well demonstrated from the TEM and HRTEM photographs presented in Figs. 1 and 3. At this stage of particle development, the particle size remains constant with time while the concentration is known to increase. This fact could also explain why the density of crystallites found in the sample deposited at T_{ON}=1 s and 100 °C is higher than at T_{ON}=5 s and 150 °C, since the T_{ON} used at 100 °C is closer to the onset time for particle coagulation than the T_{ON} used at 150 °C.

In addition, the sample deposited at 100 °C and T_{ON}=5 s may be formed by nanoparticles just after the coagulation process. This is in agreement with the TEM image of Fig. 1(c), which shows the presence of larger crystallites. The presence in this film also of the smallest particles of 1–2 nm as revealed in Fig. 2(c) is identified as a population of particles that started their growth later in the plasma-on period. Moreover, the existence of amorphous powder particles bigger in size than those shown in Figs. 1(c)–3(c) cannot be ruled out, since the contrast between them and the amorphous Si matrix is practically unobservable.

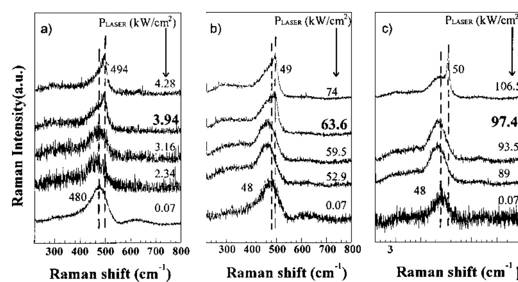

FIG. 4. Comparison between Raman measurements on pm-Si:H films [deposited at T_G=100 °C, T_{ON}=5 s (a) and T_{ON}=1 s (b)] and a standard *a*-Si:H thin film. The Raman spectra were recorded at increasing laser power densities, which are indicated on each spectrum. In both cases, the first Raman spectrum was obtained in the macro mode in order to get very low laser power density on the sample, i.e., to avoid any spurious effect on the Raman signal. The other ones were recorded in the micro mode.

It is important to remark that, for the sample deposited at 100 °C and at T_{ON}=1 s, the T_{ON} used is a little smaller than the characteristic coagulation time $t_2 \approx 2$ s. Therefore, a higher density of nanocrystallites is expected for the corresponding film obtained just before particle coagulation, and this is consistent with the higher crystalline density of the samples deposited at 100 °C and T_{ON}=5.

As a conclusion, the TEM and HRTEM analysis shown in Figs. 1–3 agrees with previous growth kinetic studies on Si nanoparticles in rf plasmas, and corroborates the hypothesis that the polymorphous films considered here come from the simultaneous deposition of radicals and particles.

B. Raman scattering

1. Laser power density for film crystallization

In order to avoid misinterpretation of the Raman spectra, Raman measurements are generally performed at a low laser power. Excessive laser irradiation could modify the shape and position of the Raman peaks due to disturbance of the interatomic potential and moreover it could result in a partial film crystallization.[16,33–35] We have thus performed a preliminary Raman analysis by increasing laser power in order to investigate the evolution of the Raman spectra with laser power, and hence, of the film structure. In addition, this analysis allows between the structure of the as-deposited thin films and the laser-induced crystallized ones to be distinguished. Figure 4 shows Raman spectra of two different pm-Si:H films [Figs. 4(a) and 4(b)] for different laser power densities. For comparison, the same analysis of a standard *a*-Si:H thin film is also presented [Fig. 4(c)]. At very low laser power, the Raman spectrum of the pm-Si:H films corresponds to an amorphous silicon film, which is characterized by a broadband at 480 cm^{-1}. However, TEM photographs of pm-Si:H films have highlighted the presence of nanocrystalline Si embedded in the amorphous silicon matrix, but with a very small crystalline density (<3%). Therefore, the crystalline Raman signal predicted for these crystallites at around 505 cm^{-1} (as calculated for Si spheres of 1.5 nm using an appropriate phonon confinement model[36]) is

Downloaded 15 Jun 2010 to 161.116.168.169. Redistribution subject to AIP license or copyright; see http://jap.aip.org/jap/copyright.jsp

negligible compared to the amorphous one at 480 cm^{-1}, thus explaining the lack of a crystalline-like peak in the corresponding Raman spectra.

The crystallization of the films at increasing Raman laser power is obvious from Fig. 4, which shows the appearance of a sharp peak superimposed on the amorphous one at the high wavelength side. Therefore, a threshold laser power (P_T) for crystallization is defined. A similar crystalline peak appears in the standard *a*-Si:H film for a higher laser power density, thus indicating a slower crystallization process in the *a*-Si:H thin film in comparison with the pm-Si:H one. This result has already been attributed to the presence of crystalline entities of 1–2 nm in the matrix of the pm-Si:H thin films acting as precursors for crystallization.[16] As a matter of fact, the sample in Fig. 4 that crystallizes more easily (film grown at 100 °C and $T_{ON}=5$ s) contains a high density of crystalline domains, as we have shown above from its TEM analysis (Figs. 1–3).

However, other authors have emphasized that changes in the film porosity and/or in the surface roughness can also influence the crystallization kinetics.[18,37,38] These aspects will be discussed below. P_T is found in all cases to be characteristic of each film structure. In the following, pm-Si:H films obtained under different plasma conditions will be analyzed by Raman spectroscopy, and the laser-induced film crystallization discussed as a function of their peculiar nanostructure.

It is important to remark that before the onset of crystallization, the amorphous peaks show a shift toward lower frequencies due to heating effects in the samples. Under these conditions the temperature reached by the sample is not enough to induce crystallization. This result is very relevant because it points out the high sensitivity of the Raman measurements to the laser power used. Great care is therefore required when the Raman spectra are interpreted. For example, a broadband between 435 and 470 cm^{-1} has already been attributed to isolated silicon nanoclusters.[39] Therefore, an amorphous Raman peak shifted to lower frequencies due to a thermal effect can give rise to an erroneous interpretation if it is believed to be due to the presence of Si clusters.

2. Evolution of laser power density for crystallization of films prepared at different T_{ON}

Figure 5 summarizes the evolution of P_T for pm-Si:H thin films deposited at different T_{ON}($0.1\ s<T_{ON}<5\ s$) and at two different gas temperatures $T_G=25$ and 100 °C. The results of Fig. 5 reveal that, for the two gas temperatures, P_T decreases when T_{ON} increases. In addition, whatever the experimental conditions used to prepare the pm-Si:H films, the laser power density necessary to induce the crystallization of the standard *a*-Si:H sample is much higher than for the pm-Si:H.

This result has been previously related to the presence of Si-ordered particles in the as-deposited pm-Si:H films acting as germs in the amorphous-to-crystalline transition, while without such nanocrystallites (typical *a*-Si:H films), higher energies are needed to start nucleation.[12,16] The TEM results presented in Sec. A provide evidence for this hypothesis. However, other reasons, such as film density and/or surface

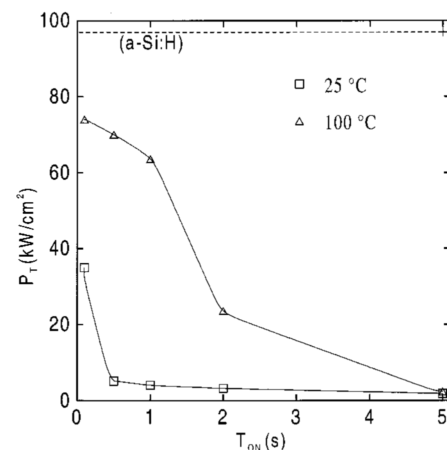

FIG. 5. Evolution of the crystallization threshold laser power density (P_T) of pm-Si:H films produced at gas temperature $T_G=25$ °C (□) and at $T_G=100$ °C (△) versus plasma duration (T_{ON}). The horizontal dashed line in the figure corresponds to the value measured in a standard *a*-Si:H.

roughness, can also influence the lowering of the crystallization threshold.[18,37,38] Figures 6 and 7 show the evolution of these parameters versus the plasma duration.

Using the previous results on particle formation in SiH_4–Ar plasmas,[31,32,40] we estimated the characteristic times for particle nucleation (t_1), coagulation (t_2), and molecular sticking (t_3) for the two deposition temperatures considered in this study (see A). At a temperature of 25 °C, $t_1\approx0.001-0.01$ s, $t_2\approx0.15$ s, and $t_3\approx4$ s, while at 100 °C, $t_1\approx0.35$ s, $t_2\approx2$ s, and $t_3\approx13$ s. In view of these results, the films deposited at 100 °C with 1 and 5 s of plasma duration (whose TEM analyses were presented in Figs. 1–3) can be compared in terms of nanoparticle contribution with the films deposited at 25 °C but using 0.1 and 0.5 s, respectively. Such a huge difference in particle development is due to the great influence of temperature on particle formation in rf plasmas.[20,40] Both at 25 and at 100 °C, the two sets of T_{ON} are found to be close to the coagulation onset, if compared with the characteristic time t_2 calculated just above for each temperature. However, for the T_{ON} periods considered in this study, only the films deposited at 25 °C illustrate the dependence of P_T on particle development when the particles are in their third growth phase.

a. pm-Si:H grown under conditions of particle nucleation. Before particle coagulation, the obtained polymorphous films deposited under these conditions (25 °C, $T_{ON}=0.1$ s; 100 °C, up to $T_{ON}=2$ s) should consist of an amorphous matrix in which monodispersed nanocrystallites of around 2 nm are embedded. This has been clearly demonstrated here by TEM for the sample deposited at 100 °C and at $T_{ON}=1$ s [Figs. 1(b), 2(b), and 3(b)]. It can therefore be asserted that there is a similar film nanostructure for the sample deposited at 25 °C and at $T_{ON}=0.1$ s. As Boufendi and Bouchoule[20] have shown, before coagulation the size of the Si crystallites remains constant and their concentration increases. As a result, the density of crystallites being incorporated into the Si growing film should increase with the T_{ON}. This result is consistent with the decrease of P_T for the films deposited at 100 °C at increasing T_{ON} up to 2 s, as shown in Fig. 5, in that the higher the density of nanocrys-

Downloaded 15 Jun 2010 to 161.116.168.169. Redistribution subject to AIP license or copyright; see http://jap.aip.org/jap/copyright.jsp

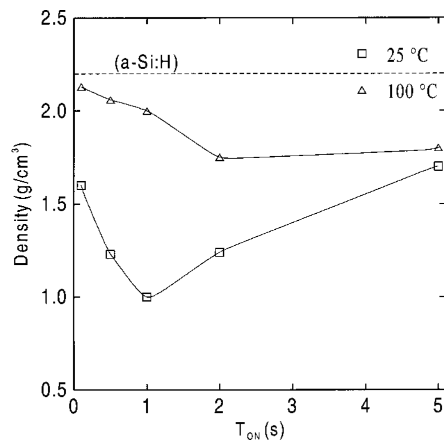

FIG. 6. Evolution of the density of pm-Si:H films produced at gas temperature $T_G = 25\,°C$ (□) and at $T_G = 100\,°C$ (△) vs plasma duration (T_{ON}). The horizontal dashed line in the figure corresponds to the value measured in a standard *a*-Si:H sample.

tallites in the films, the easier the laser induced crystallization.

In addition, the decrease in film density could also influence the film crystallization, as a consequence of a reduction in the thermal conductivity of the film (i.e., of the heat diffusion).[18] Furthermore, the excess of free energy in less dense films could also favor film crystallization. Figure 6 shows that under conditions of particle nucleation (for the samples deposited at 100 °C, up to $T_{ON} = 2$ s), the film density diminishes. The decrease in the film density is maybe due to the increase in nanoparticle concentration with plasma duration (as explained above), leading to an increase in film porosity. However, we can notice that while the *a*-Si:H film density is very similar to that of the pm-Si:H films deposited at shorter T_{ON} and at 100 °C, P_T is largely different. This result emphasizes that the presence of nanocrystallites embedded in these films may play a more important role in the crystallization process than the film density.

Changes in surface roughness can also modify the film crystallization.[18,37] Figure 7 reports the variation in surface roughness of these films. It was not possible to measure the roughness of the samples deposited at 25 °C from $T_{ON} = 0.5$ s

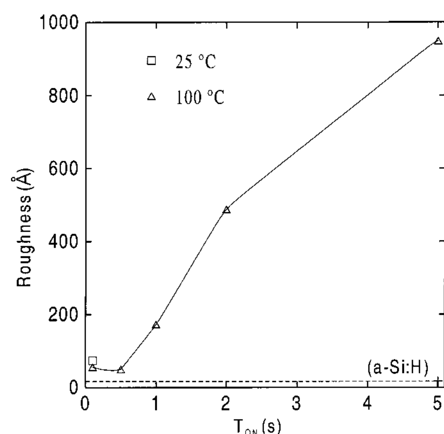

FIG. 7. Evolution of the surface roughness of pm-Si:H films produced at gas temperatures $T_G = 25\,°C$ (□) and $T_G = 100\,°C$ (△) vs plasma duration (T_{ON}). The horizontal dashed line in the figure corresponds to the value measured in *a*-Si:H.

due to the dusty character of such films. Only the value calculated for the sample at $T_{ON} = 0.1$ s is presented in Fig. 7. For the samples deposited at 100 °C using T_{ON} between 0.5 and 2 s, the surface roughness increases with T_{ON}. Previous studies have pointed out the effect of surface roughness on the film crystallization:[18,37] (i) the surface roughness can act as a seed for the crystallization; (ii) the roughness can induce a photon "trapping," and thus induce a higher surface heating; and (iii) the roughness can enhance the electromagnetic field on the surface. As a consequence, the lowering of the crystallization threshold when T_{ON} increases could also be due to the increase in surface roughness with T_{ON}. However, it is important to note that the surface roughness of the standard *a*-Si:H sample (dashed line in Fig. 6) is found to be similar to that of the pm-Si:H samples deposited at shorter T_{ON}, while the corresponding threshold laser powers measured by Raman (Fig. 5) are greatly different. This result emphasizes the role of the nanocrystallites embedded in the pm-Si:H acting as seeds for the amorphous-to-crystalline transition.

b. pm-Si:H grown under conditions of particle coagulation. Referring to the characteristic times of particle development deduced in Sec. A, the films grown under conditions of particle coagulation are: (a) at 25 °C, from $T_{ON} = 0.5$ s to $T_{ON} = 2$ s, and at 100 °C, from $T_{ON} = 2$ s to $T_{ON} = 5$ s. Figure 5 shows that P_T decreases in both cases. However, this evolution is slower than for the samples grown under conditions of particle nucleation.

Figure 7 also shows an increase in surface roughness under these plasma conditions. However, density measurements (Fig. 6) reveal that the density for the film deposited at 25 °C diminishes up to 1 s and then increases, while it remains almost constant for the films deposited at 100 °C.

In order to explain such results, the process of particle formation in the plasma can be again taken into account. Just after the onset of the particle coagulation process in the plasma, the films grow by the incorporation of particles with different diameters, as we have observed from the TEM images corresponding to the sample deposited at $T_{ON} = 5$ s and 100 °C [Figs. 1(c)–3(c)]. Similar results are then expected for the sample deposited at $T_{ON} = 0.5$ s and 25 °C. The coagulation process gives rise to the formation of larger particles in the plasma, as a result of the coalescence of smaller crystallites. These particles are incorporated into the growing film during the T_{OFF} periods. The TEM images reported in Fig. 1 showed clearly the presence of larger crystallites in the film obtained at $T_{ON} = 5$ s and 100 °C. The increase in particle size during the coagulation phase also explains the increase in surface roughness shown in Fig. 6.

These results agree with the easier crystallization of these films as shown in Fig. 5. In addition, the fact that P_T decreases slowly under these conditions is consistent with the coagulation mode itself, since, although the size of the nanoparticles does increase, their concentration is known to decrease.

The increase in particle size during coagulation should also produce a decrease in film density, since the larger the particles incorporated into the film (which increase with T_{ON}), the higher the porosity of the resulting films. However,

Downloaded 15 Jun 2010 to 161.116.168.169. Redistribution subject to AIP license or copyright; see http://jap.aip.org/jap/copyright.jsp

no appreciable changes in film density are observed for the films deposited at 100 °C between 2 and 5 s, moreover, for the films deposited at 25 °C and $T_{on}>1$ s, the density increases. This result is discussed below, taking into account the effect of plasma duration on the film microstructure. It proves, nevertheless, that there is not a clear correlation between the crystallization threshold and film density.

c. pm-Si:H grown under conditions of molecular sticking. Only the sample deposited at 25 °C and $T_{ON}=5$ s illustrates this growth mode. Figure 5 shows that P_T is almost constant under this condition, when comparing the sample deposited at $T_{ON}=2$ s and the sample deposited at $T_{ON}=5$ s. This behavior can be well correlated with the nanostructure of the films by considering the characteristics of the powders which were incorporated during their growth. For longer plasma-on times, the thin films obtained became powder-like films due to the incorporation of large powder particles (>20 nm). As discussed above, the powder density at this temporal stage remains constant. Indeed, these dust particles are known to be formed by small crystallites embedded therein. These crystallites come from the first generation of particles created just before coagulation.[20] Therefore, the density of crystallites which can serve as seeds in the amorphous-to-crystalline film transition is found to remain constant in this stage. This may explain why P_T does not change appreciably for these films.

The increase in T_{ON} does surprisingly produce an increase in the density of the obtained films, as shown in Fig. 6. This can be explained by different reasons. First during the plasma period, the growth rate of the powders which are incorporated into the film during the T_{OFF} periods is found to diminish (with respect to the coalescence phase), while the deposition rate of the continuous amorphous layer simultaneously deposited on the substrate during the T_{ON} periods could be considered constant. Second, the increase in plasma duration obviously augments the time during which the films are exposed to ion bombardment from the plasma. It is known that,[38] in discharges of SiH_4 diluted in Ar, the bombardment due to high energetic ions on the surface can produce a densification of the film microstructure and a reduction of the surface roughness (by enhancing the surface mobility and the structural rearrangement). Moreover, this can reduce the polymeric hydrogenated bonds in favor of SiH groups, thus increasing the film density. As a consequence, the density of the resulting film could increase with the T_{ON}, as can be seen in Fig. 6.

As a conclusion of this section, the lack of a clear dependence between the density of the films and their *in situ* crystallization during Raman scattering measurements emphasizes the role of the nanocrystalline character of pm-Si:H films in the crystallization process.

3. Evolution of laser power density for crystallization of films prepared at different temperatures

Figure 8 reports the evolution of P_T in pm-Si:H films as a function of the deposition temperature T_G. The plasma-on time was the same and equal to $T_{ON}=5$ s. As a comparison, the value for the standard a-Si:H is also included (for a sample deposited at 250 °C). The figure shows that P_T remains low and almost increases up to 100 °C and then strongly increases for $T_G=150$ °C. A higher crystallization threshold is measured for the standard a-Si:H.

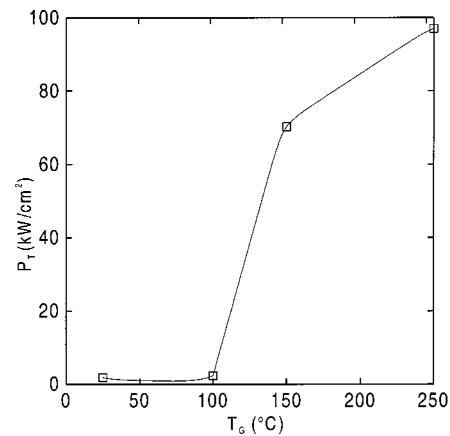

FIG. 8. Evolution of the crystallization threshold laser power density (P_T) of pm-Si:H films deposited at the same plasma duration $T_{ON}=5$ s but at different gas temperatures (T_G). The value at 250 °C corresponds to a standard a-Si:H sample.

In order to explain this evolution, the different role of the film nanostructure, film density and surface roughness can be analyzed, in the same way that we have studied the crystallization of the films as a function of plasma duration.

As discussed in Secs. A and B1, the film nanostructure depends on the set of particles that contribute to its deposition. A change in deposition temperature greatly affects particle development. For the three temperatures considered here ($T_G=25$, 100, 150 °C), the characteristic times of particle development in the plasma were calculated in Sec. A. Taking into account those results, the sample deposited at 25 °C and $T_{ON}=5$ s is a dusty-like film, the sample deposited at 100 °C and $T_{ON}=5$ s is formed by nanoparticles just after the beginning of their coagulation in the plasma [TEM images in Figs. 1(c) and 3(c)], and the sample deposited at 150 °C and $T_{ON}=5$ s should contain only nanoparticles of few nanometers which came from the first nucleation stage [TEM images in Figs. 1(a) and 3(a)]. The dusty character of the films deposited at 25 °C impeded its preparation for TEM analysis. The great difference in crystalline density found between the samples deposited at 150 and 100 °C [see Figs. 2(a) and 2(c)] could explain the huge drop in the crystallization threshold as observed in Fig. 8, since precursors for crystallization are less numerous at 150 °C and this fact increases the energy needed to start crystallization. However, the sample deposited at 25 °C is formed by big powders in which small crystallites (identified as the first generation of particles from which the coagulation started) are known to be embedded. Therefore, the density of nanocrystallites in the samples deposited at 25 and 100 °C appears to be very similar, and this can explain why P_T is almost the same for both samples.

In addition, deposition temperature can affect the film structure in different ways. Indeed, density and surface roughness evolve as a function of deposition temperature (Figs. 9 and 10), and they could also affect the film crystal-

Downloaded 15 Jun 2010 to 161.116.168.169. Redistribution subject to AIP license or copyright; see http://jap.aip.org/jap/copyright.jsp

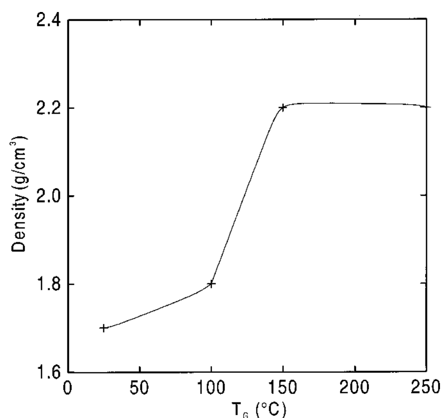

FIG. 9. Evolution of the density of pm-Si:H films deposited at the same plasma duration T_{ON}=5 s but at different gas temperature (T_G). The value at 250 °C corresponds to a standard a-Si:H sample.

lization to some extent. The following interpretations can be proposed:

First, the mobility of the species deposited on the film surface during the plasma deposition process is strongly affected by temperature. The increase in temperature enhances the structural rearrangement on the surface and this is found to improve the film microstructure. Denser films and with less surface roughness are then obtained at increasing deposition temperature. This is consistent with the results reported in Figs. 9 and 10.

Second, it is widely recognized that deposition temperature also influences both the hydrogen content of the films and the hydrogen bonding configuration. Low temperatures are related to the deposition of films with a high degree of microstructure, i.e., polymeric-like films. However, at high temperature (~250 °C), the films are grown mainly from primary reaction products, and high quality and denser amorphous films formed by monohydride Si–H in the bulk are obtained. In this way, changes in the H bonding configuration with deposition temperature can also cause changes in the film density.

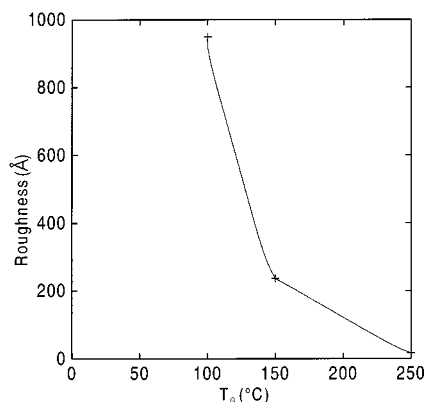

FIG. 10. Evolution of the surface roughness of pm-Si:H films deposited at the same plasma duration T_{ON}=5 s but at different gas temperature (T_G). The value at 250 °C corresponds to a standard a-Si:H sample.

As a conclusion, the increase in temperature could enhance the role of the continuous layer (deposited during the T_{ON} periods) in the properties of the whole structure, such as film density and surface roughness, and this could also influence the laser-induced crystallization observed by Raman scattering.

It is important to stress that the powder formation in the plasma gas phase, which is temperature triggered as discussed above, also modifies film density and surface roughness: the higher the size and concentration of particles in the plasma being deposited on the film, the smaller the density of the resulting films, and the higher their surface roughness.

In view of these results, the evolution of film crystallization with deposition temperature can be discussed taking into account the effect of the temperature on the process of powder formation. However, the great increase in the crystallization threshold at 150 °C observed in Fig. 8 could also be attributed to an effect of microstructure improvement at increasing deposition temperature.

Nevertheless, as shown in Fig. 9, the film density of the sample deposited at 150 °C and T_{ON}=5 s is found to be very similar to that of the a-Si:H sample, while P_T is vastly different (Fig. 8). In addition, if we compare the value of P_T for the sample deposited at 150 °C and T_{ON}=5 s (Fig. 8) with the values measured for the samples deposited at 100 °C under T_{ON}=1 s (Fig. 5), we observe that they are very similar. In contrast, the corresponding values of film density and surface roughness are different. Taking into account the characteristic times for particle development calculated in Sec. A, it is clear that nanoparticles coming from their first nucleation stage contribute to the growth of such films. Consequently, these films exhibit the same degree of nanostructure. This result is of great relevance, since it highlights the role of the nanocrystalline character of pm-Si:H films in their laser-induced crystallization during Raman scattering and demonstrates the feasibility of Raman measurements to evaluate the nanostructure of the films.

IV. CONCLUSION

Mixtures of amorphous-nanocrystalline Si thin films have been grown from Ar-diluted SiH_4 rf plasmas under dust-forming conditions. TEM analysis has evidenced this peculiar film structure and has demonstrated the connection between the Si crystallites embedded in the films and the nanorparticles formed in the plasma gas phase during film deposition. In addition, from electron diffraction, the Si nanocrystallites are shown to present a face-centered-cubic structure, different both from the diamond-like structure in c-Si and from other metastable structures found in Si clusters. This is currently being investigated and will be developed in a separate article.

The recrystallization of these thin films, called polymorphous Si (pm-Si:H), has been investigated *in situ* using Raman scattering. The role of different films properties, such as surface roughness, film density, and nanocrystallite volume fraction, in the film crystallization has been carefully studied. The results have shown that the presence of crystallites embedded in the amorphous matrix of the pm-Si:H films plays a

Downloaded 15 Jun 2010 to 161.116.168.169. Redistribution subject to AIP license or copyright; see http://jap.aip.org/jap/copyright.jsp

determining role in this process. However, they also emphasize that film density does not have a dominant effect in the recrystallization phenomenon.

ACKNOWLEDGMENTS

This study was financed by the European Community under Contract ''H-Alpha Solar'' No. ERK6-CT-1999-00004 and partially supported by CICYT, MAT99-0569-CO2-01 of the government of Spain. The authors thank Professor Pere Roca i Cabarrocas for the preparation of *a*-Si:H samples. Thanks also to Elizabeth Jolivet for English language corrections, Henriette Estrade for AFM measurements, and to Juan Carlos Ferrer (from the Serveis Cientifico-Tecnics of the University of Barcelona) for his help with the TEM measurements.

[1] *Amorphous Silicon Technology-1992*, edited by A. Madan, Y. Hamakawa, M. J. Thompson, P. C. Taylor, and P. G. LeComber (Materials Research Society, Pittsburgh, 1991, R. A. Street, MRS Bulletin XVII 1992), Vol. 70.
[2] Ch. Steinbrüchel, in *Physics of Thin films*, edited by M. H Francombe and J. L. Vossen (Academic, New York, 1994), Vol. 11, p. 289.
[3] N. Hershkowitz (Ed.), Plasma Sources Sci. Technol. **3**, 239 (1994).
[4] R. N. Carlile, J. Vac. Sci. Technol. A **14**, 487 (1996).
[5] *Dusty Plasmas, Physics, Chemistry and Technological Impacts in Plasma Processing*, edited by A. Bouchoule (Wiley, New York, 1999).
[6] C. Longeaud, J. P. Kleider, P. Roca i Cabarrocas, S. Hamma, R. Meaudre, and M. Maudre, J. Non-Cryst. Solids **227–230**, 96 (1998).
[7] M. Meaudre, R. Meaudre, R. Butté, S. Vignoli, C. Longeaud, J. P. Kleider, and P. Roca i Cabarrocas, J. Appl. Phys. **86**, 946 (1999).
[8] J. P. Kleider, C. Longeaud, M. Gauthier, M. Meaudre, R. Meaudre, R. Butté, S. Vignoli, and P. Roca i Cabarrocas, Appl. Phys. Lett. **75**, 3351 (1999).
[9] R. Butté, R. Meaudre, M. Meaudre, S. Vignoli, C. Longeaud, J. P. Kleider, and P. Roca i Cabarrocas, Philos. Mag. B **79**, 1079 (1999).
[10] P. Roca i Cabarrocas, Appl. Phys. Lett. **65**, 1674 (1994).
[11] P. Roca i Cabarrocas, P. Gay, and A. Hadjadj, J. Vac. Sci. Technol. A **14**, 655 (1996).
[12] E. Bertran, S. N. Sharma, G. Viera, J. Costa, P. St'ahel, and P. Roca i Cabarrocas, J. Mater. Res. **13**, 2476 (1998).
[13] P. Roca i Cabarrocas, Mater. Res. Soc. Symp. Proc. **507**, 855 (1998).
[14] P. Roca i Cabarrocas, J. Non-Cryst. Solids **266–269**, 31 (2000).
[15] R. Butté, S. Vignoli, M. Meaudre, R. Meaudre, O. Marty, L. Saviot, and P. Roca i Cabarrocas, J. Non-Cryst. Solids **266–269**, 263 (2000).
[16] G. Viera, P. Roca i Cabarrocas, J. Costa, S. Martinez, and E. Bertran, Mater. Res. Soc. Symp. Proc. **507**, 933 (1998).
[17] J. Costa, P. Roura, P. Roca i Cabarrocas, G. Viera, and E. Bertran, Mater. Res. Soc. Symp. Proc. **507**, 499 (1998).
[18] A. Hadjadj, L. Boufendi, S. Huet, S. Schelz, P. Roca i Cabarrocas, H. Estrade-Szwarckopf, and B. Rousseau, J. Vac. Sci. Technol. A **18**, 529 (2000).
[19] A. Bouchoule, A. Plain, L. Boufendi, J. Ph. Blondeau, and C. Laure, J. Appl. Phys. **70**, 1991 (1991).
[20] L. Boufendi and A. Bouchoule, Plasma Sources Sci. Technol. **3**, 262 (1994).
[21] P. Roca i Cabarrocas, J. B. Chévrier, J. Huc, A. Lloret, J. Y. Paret, and J. P. M. Scmitt, J. Vac. Sci. Technol. A **9**, 2331 (1991).
[22] G. Viera, E. García-Caurel, J. Costa, J. L. Andújar, and E. Bertran, Appl. Surf. Sci. **144**, 702 (1999).
[23] J. R. Chelikowsky and J. C. Phillips, Phys. Rev. Lett. **63**, 1653 (1989).
[24] M. V. Ramakrishna and J. Pan, J. Chem. Phys. **101**, 8108 (1994).
[25] J. Pan and M. V. Ramakrishna, Phys. Rev. B **50**, 15431 (1994).
[26] U. R. Röthlisberger, W. Andreoni, and M. Parinello, Phys. Rev. Lett. **52**, 665 (1994).
[27] H. Hofmeister, J. Dutta, and H. Hofmann, Phys. Rev. B **54**, 2856 (1996).
[28] G. K. Ramachandran, J. Diefenbacher, O. F. Sankey, R. Sharma, R. F. Marzke, M. O'Keeffe, J. Gryko, and P. F. McMillan, Mater. Res. Soc. Symp. Proc. **507**, 483 (1998).
[29] H. Kawaji, H. Horie, S. Yamanaka, and M. Ishikawa, Phys. Rev. Lett. **74**, 1427 (1995).
[30] G. Viera G. and L. Boufendi (unpublished).
[31] L. Boufendi, J. Herman, A. Bouchoule, B. Dubreil, E. Stoffels, W. W. Stoffels, and M. L. deGiorgi, J. Appl. Phys. **76**, 148 (1994).
[32] L. Boufendi, G. Viera, and G. J. Gaudin (unpublished).
[33] T. R. Hart, R. L. Aggarwal, and B. Lax, Phys. Rev. B **1**, 638 (1970).
[34] R. Tsu and J. G. Hernandez, Appl. Phys. Lett. **41**, 1016 (1982).
[35] G. Viera, S. Huet, and L. Boufendi (unpublished).
[36] J. Zi, H. Büscher, C. Falter, W. Ludwing, K. Zhang, and X. Xie, Appl. Phys. Lett. **69**, 200 (1996).
[37] A. Hadjadj, A. Beorchia, L. Boufendi, S. Huet, and P. Roca i Cabarrocas, J. Vac. Sci. Technol. A **19**, 124 (2001).
[38] A. Hadjadj, A. Beorchia, P. Roca i Cabarrocas, L. Boufendi, S. Huet, and J. L. Bubendorff, J. Phys. D **34**, 1 (2001).
[39] E. C. Honea, A. Ogura, D. R. Peale, C. Félix, C. A. Murray, K. Raghvachari, W. O. Sprenger, M. F. Jarrold, and W. L. Brown, J. Chem. Phys. **110**, 12 (1999).
[40] L. Boufendi, A. Bouchoule, and T. Hbid, J. Vac. Sci. Technol. A **14**, 572 (1996).

Downloaded 15 Jun 2010 to 161.116.168.169. Redistribution subject to AIP license or copyright; see http://jap.aip.org/jap/copyright.jsp